THE JOURNAL OF PHYSICAL CHEMISTRY C

ARTICLE

pubs.acs.org/JPCC

Effect of Annealing Temperature on TiO_2−ZnO Core−Shell Aggregate Photoelectrodes of Dye-Sensitized Solar Cells

Kwangsuk Park, Qifeng Zhang, Betzaida Batalla Garcia, and Guozhong Cao*

Department of Materials Science and Engineering, University of Washington, Seattle, Washington 98195, United States

Supporting Information

ABSTRACT: Photoelectrodes made of submicrometer-sized aggregates of ZnO nanocrystallites coated with TiO_2 layer by atomic layer deposition with different annealing temperatures were investigated for dye-sensitized solar cells. Although the annealing at 350 °C is commonly used for the ZnO aggregates in order to preserve the desired large surface area and mesoporous structure, the presence of ALD-TiO_2 layer on the ZnO aggregates would enable to increase the annealing temperature up to 450 °C without a loss of surface area by suppressing surface diffusion of the ZnO atoms. The morphology and crystal size of the aggregates and BET results supported the fact that ALD-TiO_2 layer coated on the ZnO aggregates is effective in preventing the surface diffusion of the ZnO atom at elevated annealing temperature. Electrochemical property of the photoelectrodes including the charge transfer resistance was significantly affected by the annealing temperature. Electrochemical impedance spectroscopy revealed that the charge transfer resistance at the ZnO aggregate/electrolyte interface, where recombination occurs, increased with the annealing temperature. The larger charge transfer resistance is thought to reduce the surface recombination and thus contributes to the increase in the open circuit voltage (V_{oc}) of the DSCs as much as ∼100 mV. The increase in fill factor as well as V_{oc} of the cell was observed corresponding to the increasing annealing temperature, and these improvements finally lead to more than 30% enhancement in the efficiency of DSCs.

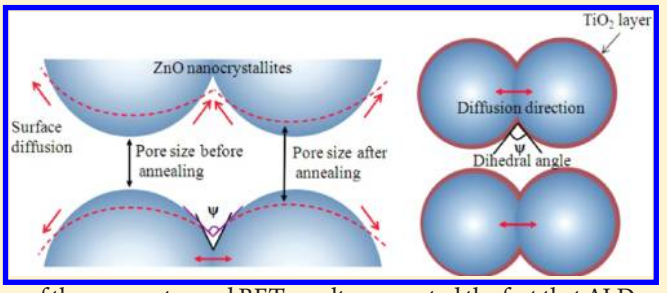

INTRODUCTION

Dye-sensitzed solar cells (DSCs) have been considered as an alternative to silicon-based solar cells, which have been commercialized for more than 50 years, due to their low cost and unique characteristics such as transparency.[1,2] However, there are still remaining challenges to widely apply them in our daily life, such as relatively low power conversion efficiency and long-term reliability. Since the efficiency of 11% was achieved, lots of efforts have been focused on the further improvement of the DSC performance but little progress has been made.[3,4]

The nanoporous film of semiconductor materials with a wide band gap, used as a photoelectrode of DSCs, is a crucial part of the DSCs in achieving high power conversion efficiency, because it provides the large surface area for adsorbing sufficient dye molecules for photon capturing and electron−hole pair generation. However, the huge surface area of the nanoporous network makes the charge recombination at the interface a viable concern.[5] The charge recombination process, which is recognized as one of the main issues to deteriorate the power conversion of the DSCs, is known to occur by transferring the electrons in the nanoporous semiconductor network not only to the oxidized ions in the electrolyte that is in direct contact with the semiconductor surface, but also to the oxidized dye molecules adsorbed on the surface of the semiconductor.[6,7]

Lots of effort have been made to prevent or reduce the charge recombination by applying a core−shell configuration.[8−10] When the materials for the shell and core are selected and the shell is appropriately fabricated, such a structure is expected to suppress the recombination process by forming an energy barrier to prevent the electrons in the conduction band of the semiconductor from transferring to the oxidized dyes and ions in the electrolyte, leading to increased open circuit voltage and short current density.[11]

For the fabrication of the thin conformal coating on nanoporous photoelectrodes of DSCs, atomic layer deposition (ALD) has been considered as one of the favorite methods because it offers precise control of the thickness and conformal coating at relatively low temperature,[12,13] and many semiconductor materials such as TiO_2, ZnO, SnO, and Al_2O_3 have been successfully deposited on nanoporous materials.[10,14,15] In our previous work, the TiO_2 ultrathin layer (<1 nm) was successfully coated onto the exposed surface of the submicrometer aggregates of ZnO nanocrystallites by ALD and resulted in a 20% increase in the overall power conversion efficiency.[16] At that time, only the annealing temperatures of 400 °C was used to get a crystalline ALD-TiO_2 layer coated on the ZnO aggregate and the effect of the ALD-TiO_2 coating on performance of DSCs was investigated. However, the ALD-TiO_2 coating on the ZnO aggregate can affect physical properties of the ZnO aggregate against the annealing temperature so that the annealing temperature itself

Received: November 14, 2010
Revised: January 23, 2011
Published: February 25, 2011

would be a crucial factor in determining the performance of the ZnO core-TiO_2 shell system.

The present paper reports a systematic experimental study on the effect of annealing temperature on the ZnO core - TiO_2 shell structures used for the photoelectrode of the DSCs in terms of physical and electrochemical aspects. The annealing at 350 °C prefers for the ZnO aggregates to preserve their huge surface area because high annealing temperature induces severe sintering of the ZnO nanocrystallites, resulting in the reduction of surface area. In the ZnO core−TiO_2 shell system, it is expected that the presence of the TiO_2 shell layer on the surface of the ZnO core makes it possible to change annealing temperatures without any impact on the surface area and improve performance of DSCs with the different annealing temperatures.

EXPERIMENTAL PROCEDURE

Synthesis of ZnO Aggregate. ZnO aggregates were prepared by hydrolysis of 0.01 M of zinc acetate dihydrate in diethylene glycol at 160 °C as reported previously.[18] The zinc acetate started to be dissolved around 130 °C, and then the reaction occurred after about 20 min after the dissolution of the zinc acetate, accompanied by a color change of the solution from transparent to white. The ZnO colloidal solution continued to be refluxed for 2 h. The ZnO aggregates were separated from the solvent by using a centrifuge at 6000 rpm for 20 min, followed by cleaning with ethanol. The resultant ZnO aggregates were redispersed in 5 mL of ethanol by sonication for about 10 min.

Fabrication of ZnO Film. A drop cast method was used to make ZnO films on a FTO glass. Several drops of the ZnO aggregate solution were placed on the FTO glass which has already dammed with a scotch tape. After complete evaporation of the ethanol, leaving the ZnO film on the FTO glass, the ZnO film was annealed at 350 °C for 1 h to remove organic residues and improve a connection among the ZnO aggregates and the adhesion of ZnO film on FTO substrate. The film area is 0.49 cm^2.

TiO_2 ALD Coating. Titanium isopropoxide ($Ti(OCH(CH_3)_2)_4$) and distilled water were chosen as a precursor and an oxidant for ALD-TiO_2 deposition. After connecting them to each valve, the precursor was heated at 50 °C and the oxidant was kept at 25 °C. The annealed ZnO film placed on a heater located in a vacuum chamber was heated at 220 °C under vacuum condition. One cycle of ALD is composed of (1) the precursor exposure, (2) purge the precursor remaining in the chamber, (3) the oxidant exposure, and (4) purge the residual oxidant. The ZnO film was exposed to those gaseous chemicals alternatively and after one cycle, thin TiO_2 layer was formed on the surface of the ZnO aggregates. Nitrogen gas was used as a carrier gas to deliver the precursor and oxidant effectively. After the ALD process of 10 cycles, the TiO_2 coated ZnO film was reannealed at 350, 400, and 450 °C both to achieve crystalline TiO_2 and to remove residues formed during the ALD process.

Solar Cell Fabrication. The TiO_2 coated ZnO film was sensitized with 0.3 mM *cis*-diisothiocyanato-bis(2,2′-bipyridyl-4,4′-dicarboxylato) ruthenium(II)-bis-tetrabutylammonium (commercially known as N719, Solaronix) in ethanol for 60 min. Next, the sensitized films were ringed with ethanol to remove excess dye adsorbed on the surface of the films. The sensitized films as a working electrode were assembled with a counter electrode for which a platinum-coated silicon wafer was used. These two electrodes were separated by a spacer with a thickness of 30 μm, where the I^-/I_3^- electrolyte was introduced by a capillary force. The electrolyte is composed of 0.6 M tetrabutylammomium iodide, 0.1 M lithium iodide, 0.1 M iodine, and 0.5 M 4-tert-butylpyridine in acetonitrile.

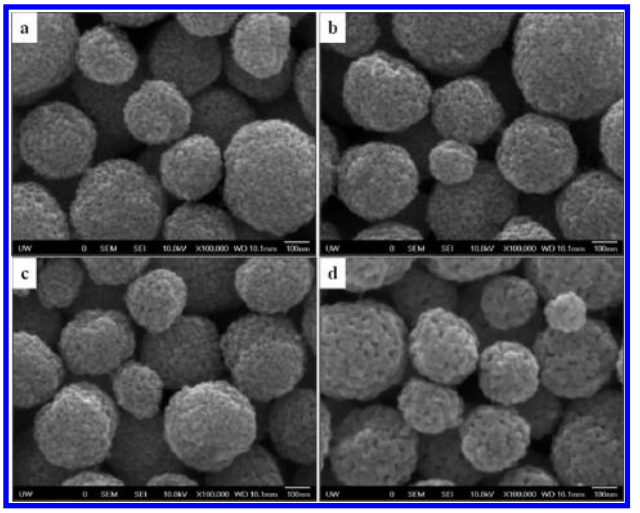

Figure 1. SEM images showing the surface morphology of submicrometer-sized aggregates of ALD-TiO_2 coated ZnO annealed at (a) 350, (b) 400, and (c) 450 °C and (d) ZnO annealed at 450 °C.

Characterization. The morphology of the TiO_2 coated ZnO aggregates was studied through Scanning electron microscopy (SEM, JSM-7000). Compositional analysis of X-ray photoelectron spectroscopy (XPS) was used to calculate the thickness of the ALD-TiO_2 layer. Brunauer−Emmett−Teller (BET) was carried out to check the surface area and sintering behaviors of the ZnO atoms during the annealing, by considering the change in the size of micropores existed in the ZnO aggregates. X-ray diffraction (XRD) with Cu Kα radiation (=0.15418 nm) was used to characterize crystallinity and crystallite size of the sample annealed with different temperature. Transmission electron microscopy (TEM, Tecnai G2 F20) was used to characterize morphology of ZnO nanocrystallites. Electrochemical impedance spectroscopy (EIS) measurement was performed by the Solartron 1287A equipped with the Solartron 1260 FRA/impedance analyzer. The bias voltage and AC amplitude applied were 0.65 V and 10 mV and the frequency ranged from 0.05 to 10^5 Hz. The performance of the solar cells was measured using the HP 4155A programmable semiconductor parameter analyzer under AM 1.5 simulated sunlight with the power density of 100 mW cm^{-2}.

RESULTS AND DISCUSSION

Figure 1 are the SEM images showing the surface morphologies of the ZnO aggregates coated with TiO_2 layer by 10 cycled ALD, followed with annealing at 350, 400, and 450 °C, and the ZnO aggregates without ALD TiO_2 coating but annealed at 450 °C. As ALD process was applied after forming a ZnO aggregate network through preannealing at 350 °C, the coated ALD-TiO_2 layer could cover the exposed part of the ZnO aggregate network where the precursor and oxidant of the ALD process can diffuse and adsorb, like surface and inside pores of the ZnO aggregates and finally, the whole exposed area of ZnO core, except for connected areas of necks between aggregates and nanocrystallites, was covered with the ALD-TiO_2 shell. The aggregates, themselves, have almost the same morphologies for all tested conditions; sizes in the range of 100−500 nm and spherical shape regardless of ALD application and

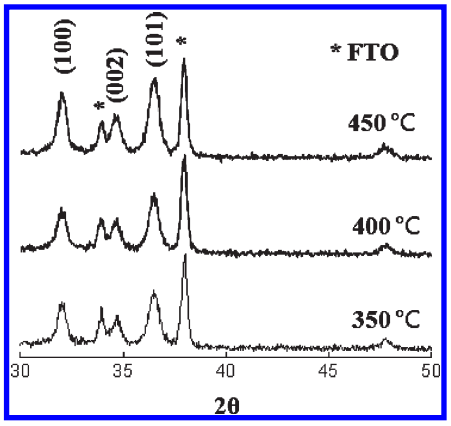

Figure 2. XRD patterns of ALD-TiO_2 coated submicrometer-sized aggregates of ZnO nanocrystallites annealed at 350, 400, and 450 °C.

Table 1. Multi-Point BET Surface Area of Submicrometer-Sized Aggregates of ALD-TiO_2 Coated ZnO Annealed at 350, 400, and 450 °C and ZnO Annealed at 450 °C

	surface area (m^2/g)
ALD-ZnO-350 °C	69.8
ALD-ZnO-400 °C	68.1
ALD-ZnO-450 °C	65.6
ZnO-450 °C	57.5

annealing temperature. However, when considering the ZnO nanocrystallites in the aggregate, different morphologies were observed. While all ALD-TiO_2 coated ZnO aggregates annealed at different temperatures still have the same morphology of the ZnO nanocrystallites, the ZnO aggregate without ALD-TiO_2 coating appears to have bigger ZnO nanocrystallites and gaps between the ZnO nanocrystallites than those of the ALD-TiO_2 coated ZnO aggregates.

It was reported that the annealing temperature over 350 °C induces a coalescence of the ZnO nanocrystallites and finally results in the reduction in the surface area of the aggregates, which would damage the performance of DSCs because an amount of the adsorbed dye is directly related to the surface area of the ZnO aggregates.[17,19] So, the annealing at 350 °C prefers to preserve the surface area of the ZnO aggregates for the high performance of the solar cells with the ZnO aggregate electrode. However, the coating of TiO_2 layer by ALD on the surface of the ZnO aggregates, even if the thickness of the TiO_2 layer applied to the ZnO aggregate is extremely thin (the thickness of the ALD-TiO_2 layer calculated by XPS compositional data is about 0.1−0.2 nm, which is an acceptable value based on the growth rate of 0.02−0.03 nm reported in the literatures)[20,21] makes it possible to maintain the surface area of the aggregates against the higher annealing temperature up to 450 °C, as shown in Figure 1a−c. No coalescence among the ZnO nanocrystallites in the aggregate was detected as the annealing temperature for the ZnO aggregates coated with TiO_2 was increased up to 450 °C. The presence of TiO_2 layer on the surface of the ZnO aggregates would prevent surface diffusion of ZnO atoms required for the coalescence of the ZnO nanocrystallites. So, the annealing temperature up to 450 °C would be applicable without any consumption of the surface area when the ZnO aggregate is coated with the ALD-TiO_2 due to the suppressed surface diffusion. The results of X-ray diffraction

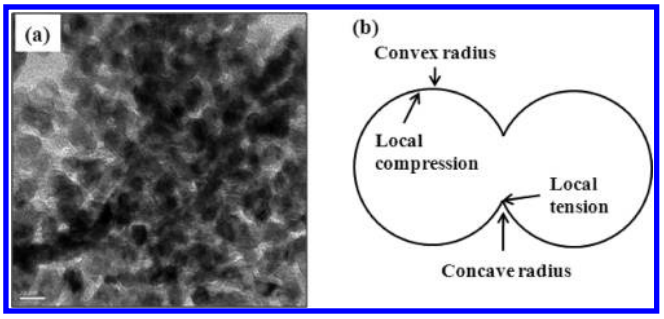

Figure 3. (a) TEM image of the microtomed ZnO aggregate showing the ZnO nanocrystallites sintered at 350 °C and (b) schematic picture showing possible stress states causing mass transport in initial sintering stage of two spherical particles. Compressive stress at a convex surface and tensile stress at a concave surface are formed.[22] The scale bar is 20 nm.

(XRD) analysis presented in Figure 2 also supported that no coalescence of ZnO nanocrystallites in the ALD-TiO_2 coated ZnO aggregates occurred with increasing the annealing temperature as well as no evidence of the ALD-TiO_2 layer because its thickness is too thin to be detected by XRS. Only the characteristic peaks of ZnO in the wurtzite crystal structure were observed for all ALD-TiO_2 coated ZnO aggregates.

According to the Scherer formula, all ALD-ZnO samples had same crystal size, ∼ 12 nm, regardless of the different annealing temperature. However, the crystal size of uncoated ZnO aggregates annealed at 450 °C was ∼14 nm as a result of the coalescence of the ZnO nanocrystallites, which is in good agreement with the SEM observation. (See Figure S1 in the Supporting Information.) The growth of the ZnO nanocrystallites would affect surface area of the ZnO aggregates and BET was used to find out variation of the surface area with different annealing temperatures. As shown in Table 1, the surface area of the ALD-ZnO aggregates was held with the annealing temperature, while the reduction in the surface area of the ZnO aggregate without the ALD-coating occurred when annealed at 450 °C due to the coalescence of the ZnO nanocrystallites as observed in the SEM and XRD results.

The presence of the ALD-TiO_2 layer on the ZnO aggregate seems to be effective in preserving the surface area of the aggregate when subjected to annealing at high temperatures. Six % loss of the surface area was observed in the ALD-TiO_2 coated ZnO aggregate annealed at 450 °C, while the ZnO aggregate without ALD-TiO_2 coating experienced much significant specific surface area reduction of ∼18% when annealed at 450 °C. So, the high annealing temperature could be applicable to ZnO aggregate when ALD-TiO_2 is applied, without detectable loss of specific surface area.

The morphology difference in the ZnO aggregates with and without ALD-TiO_2 coating might be attributed to the different sintering behavior when annealed at elevated temperatures. As shown in Figure 3a, the ZnO aggregates consist of connected ZnO nanocrystallites with a large specific surface area (∼70 m^2/g when annealed at 350 °C), and there are lots of pores between ZnO nanocrystallites within aggregates. Such a structure would undergo sintering during the annealing at elevated temperatures and thus, induce the reduction in specific surface area. At relatively low temperatures as applied in the present study, the sintering through surface diffusion and/or bulk diffusion would be predominant; compressive stress at a convex surface would

Table 2. DA Analysis Results on Pores in the Region of Micropores for the ZnO Aggregates and ALD-TiO_2 Coated ZnO Aggregates with Different Annealing Temperatures

	diameter (nm)	volume (cc/g)
ZnO − 350 °C	2.05	0.035
ALD-ZnO − 350 °C	1.96	0.031
ZnO − 450 °C	2.36	0.029
ALD-ZnO − 450 °C	1.92	0.027

promote the mass diffusion to the concave surface at the bottleneck under tensile stress, as shown in Figure 3b.[22] The diffusion of ZnO from the convex surface to the concave surface would flat the surface, resulting in a reduced specific surface area and the increased gap (the aperture size) between particles. In Figure 3(a), lots of sintered ZnO nanocrystallites with the increased neck were observed when annealed at 350 °C as a result of the mass transport caused by the different stress states.

By using Dubinin−Astakhov (DA) method as one of analysis methods in BET, only pores below the size of 5 nm which are considered to be existed in the aggregates were analyzed, as they were mostly affected by annealing at low temperatures. Pore size distributions calculated from nitrogen desorption isotherms based on the DA model gave more clear situation occurring during annealing, as shown in Table 2 and Figure 4. The ZnO aggregates annealed at 350 °C had pores with the average size of 2.05 nm, while the size of the pores in the ALD-TiO_2 coated ZnO aggregates annealed at 350 °C appeared to be 1.96 nm, indicating that the introduction of ALD-TiO_2 layer results in the size reduction of the pores for the ALD-TiO_2 coated ZnO aggregates. As the annealing temperature was increased up to 450 °C, an additional reduction in both pore size and pore volume was observed for the ALD-TiO_2 coated ZnO aggregates. On the other hand, the pores in the ZnO aggregates became larger when they were annealed at 450 °C as a consequence of sintering. It should be noted that the sintering by surface diffusion alone would result in a reduction of surface area, an increase of pore size, but no change of pore volume. However, in the present study, 17% reduction of pore volume was observed in comparison of ZnO aggregates annealed at 350 and 450 C, which suggests that there was noticeable densification through the bulk diffusion.[22]

The BET analyses suggested that there was a reduction in pore volume as well as specific surface area with the annealing temperature. Further comparison of reduction of pore volume data reveals that there was a less densification in ALD-TiO_2 coated ZnO aggregates (with ∼12% reduction viz ∼17%), suggesting that the presence of ALD-TiO_2 coating, albeit very thin, less than 1 nm, not only suppressed the sintering through the surface diffusion, but may also retarded the densification through the bulk diffusion. Densification would accelerate as a dihedral angle of two particles reaches equilibrium state, which involves surface diffusion.[23] As already discussed, the ALD-TiO_2 coating on ZnO aggregates suppresses surface diffusion so the densification would be retarded because a dihedral angle would be fixed, not to reach an equilibrium state due to the suppressed surface diffusion.

Except the sample of ZnO annealed at 450 °C, other three samples showed a similar pore size distribution, indicating that they experienced a similar sintering, even at different annealing temperature. The pore size reduction observed in the ALD-ZnO annealed at 350 °C compared to the ZnO aggregate annealed at the same temperature came from the introduction of the ALD-TiO_2 layer on the wall of the inner pores and the further size reduction with the annealing temperature was attributed to the partial sintering with densification, resulting in the pore volume reduction as well. On the other hand, the ZnO annealed at 450 °C showed the increased pore size, indicating that a different sintering behavior occurred during the annealing. Figure 5 explains schematically how the pore size changed when annealed at elevated temperatures and the difference in predominant diffusion mechanisms in ZnO aggregates with and without ALD-TiO_2 coating. At elevated temperatures, nanostructured or porous materials are subjected to sintering in order to reduce the surface area and thus the surface energy; three sintering mechanisms are well established: sintering without densification through surface diffusion at relatively low temperatures, sintering with densification through bulk or volume diffusion at moderate temperatures, and grain growth through diffusion across grain boundaries at high temperatures.[22] In the presence study, the annealing temperatures are relatively low, only surface and bulk diffusion is possible.

Once the spherical ZnO nanocrystallites experienced sintering under relatively low temperature, the neck growth occurs by the surface diffusion instead of the bulky diffusion, accompanying with increasing the dihedral angle and finally reaching the equilibrium state because making surface curvature flatted is much effective way to reduce surface energy and finally, induces the increase in the size of pores, as represented in Figure 5a. The suppressed surface diffusion due to the presence of the ALD-TiO_2 layer on the surface of the ZnO nanocrystallites would make atomic mass transport path for the sintering changed to bulky diffusion occurring at the connection part of the ZnO nanocrystallites from the surface diffusion with the preservation of the dihedral angle (ψ), as schematically shown in Figure 5b. The bulky diffusion of the ALD-TiO_2 coated ZnO, even though it would be dominant diffusion path due to the suppressed surface diffusion, induced less densification of the ZnO nanocrystallites than that of the ZnO nanocrystallites without ALD as curvature-driven boundary motion for rapid densification was prevented by the fixed dihedral angle.[23]

While the annealing temperature did not affect the physical properties of the ALD-TiO_2 coated ZnO aggregate like morphology and crystallinity, an electrochemical property, a charge transfer resistance of the ALD-TiO_2 coated ZnO photoelectrode, was considerably influenced by the annealing temperature. Electrochemical impedance spectroscopy (EIS) analysis carried out to find out the effect of the annealing temperature on the charge transfer resistance and Figure 6 shows the Nyquist plots of the EIS results including various resistance elements for the cells with ALD-TiO_2 coated ZnO aggregate photoelectrodes annealed at different temperatures. Generally, DSCs have three semicircles in the EIS Nyquist plot and each of them is related to the charge transfer at the different positions; the redox reaction at the platinum counter electrode/electrolyte interface at high frequencies (R2), the electron transfer in the aggregate film and at the aggregates/electrolyte interface at medium frequency (R3) and carrier transport by ions in the electrolyte at low frequency.[25,26] But, in this study, the EIS test was stopped after getting the second semicircle as the second semicircle is related to the charge transfer resistance at the aggregate/electrolyte interface where the ALD-TiO_2 layer was introduced.

It can be said that the ZnO core is the whole ZnO aggregate network film, not each ZnO aggregate because the core−shell

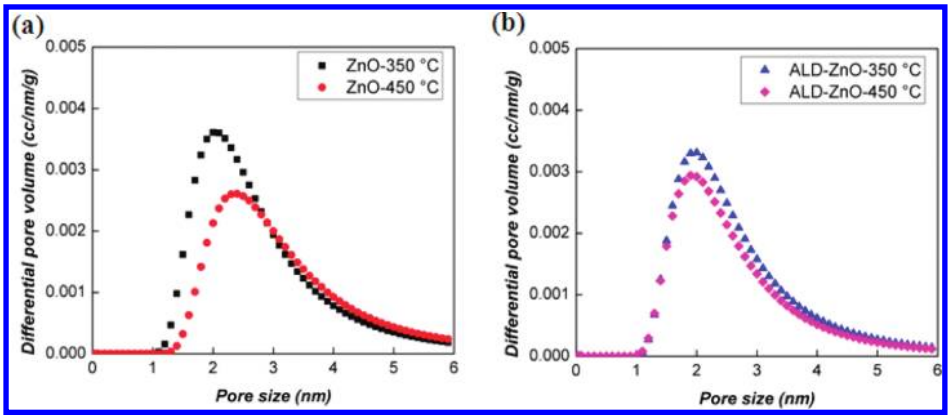

Figure 4. Pore size distribution of (a) the ZnO and (b) ALD-TiO_2 coated ZnO samples annealed at respective 350 and 450 °C calculated from nitrogen sorption isotherms measured at 77 K using the DA model.[24].

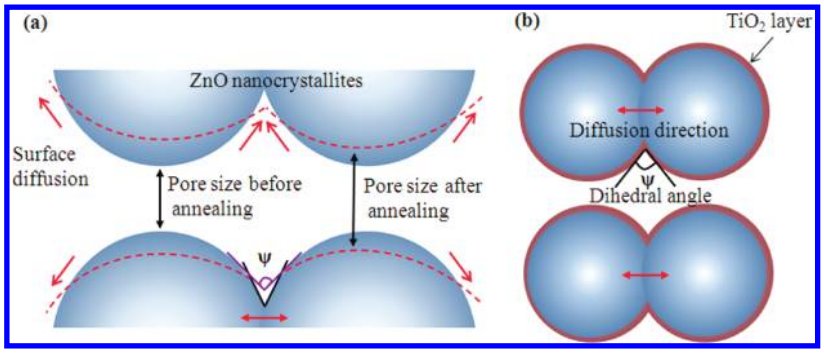

Figure 5. Schematics illustrating (a) the growth of pore by the surface diffusion of the ZnO nanocrystallites as well as the densification with increasing dihedral angel and (b) possible diffusion path and dihedral angle (ψ) kept unchanged for the TiO_2 coated ZnO nanocrystallites.

structure in this study was achieved by coating the TiO_2 layer on the preformed ZnO aggregate network. That means the increase of R3 with the annealing temperature shown in Figure 6 would be ascribed to the charge transfer resistance variation at the aggregate/electrolyte interface where the recombination occurs, not to diffusion resistance of the aggregate film because the ZnO aggregate network as an electron path did not experience any change with the annealing temperature. So, R2 and R3 denoted in the plot as diameters of the semicircles are the charge transfer resistances at the different interfaces and R1 is the ohmic resistance mainly caused by sheet resistance of the FTO glass. As the charge transfer resistances coexist with capacitance element, they have the shape of the semicircle, while the ohmic resistance, denoted as the distance from the zero point to the starting point of the first semicircle in the Nyquist plot is just a straight line because there is no capacitance element in the ohmic resistance. It is easily achieved to fit the measured data with the equivalent circuit which is a combination of the resistances and capacitances and Table 3 summarizes the fitted results for R2 and R3 with the annealing temperature.

As the charge transfer resistance at the aggregate/electrolyte interface (R3) includes the resistances of both the ZnO core and TiO2 shell, the total charge transfer resistance for the core−shell structure can be written by eq 1[27]

$$R_{\text{total}} = R_{\text{core}} + R_{\text{shell}} \quad (1)$$

where R_{core} and R_{shell} are the electron transfer resistances induced by the core and shell, respectively. From the eq 1, the increase in the total charge transfer resistance would be expected through the introduction of ALD-TiO_2 on the ZnO aggregate, but, the total charge transfer resistance of the ALD-TiO_2 coated ZnO at the aggregate/electrolyte interface was almost same to that of the ZnO aggregates when the annealing temperature was 350 °C. As-grown ALD-TiO_2 layer was proven to be amorphous and kept the amorphous phase up to the annealing at 250 °C.[10,28] From the impedance results, it can be inferred that the annealing temperature of 350 °C is not enough to transform the amorphous ALD-TiO_2 shell to the crystalline form, which would be necessary to form the ALD-TiO_2 energy barrier and the amorphous ALD-TiO_2 has no contribution to the charge transfer resistance. When the annealing temperature reaches at 400 °C, it is possible to achieve the transformation of the ALD-TiO_2 from amorphous to crystalline.[21,28] The crystalline ALD-TiO_2 increased the charge transfer resistance at the medium frequency (R3), leaving the first semicircle at the high frequency denoting the charge transfer resistance at the counter electrode/electrolyte interface (R2) unchanged. Further raising the annealing temperature up to 450 °C resulted in the additional increase in R3 because of the improved crystallinity of the ALD-TiO_2. The charge transfer resistance at the aggregate/electrolyte almost doubled as the annealing temperature increased from 350 to 450 °C, which means higher annealing temperature would be helpful in suppressing the recombination occurring at the aggregate/electrolyte interface and it can also be expected that an open circuit voltage (V_{oc}) of the DSCs would be increased by the increased the annealing temperature.

The performance of the DSCs with the working electrode consisting of the ALD-TiO_2 coated ZnO aggregates annealed at

dx.doi.org/10.1021/jp110872k |J. Phys. Chem. C 2011, 115, 4927–4934

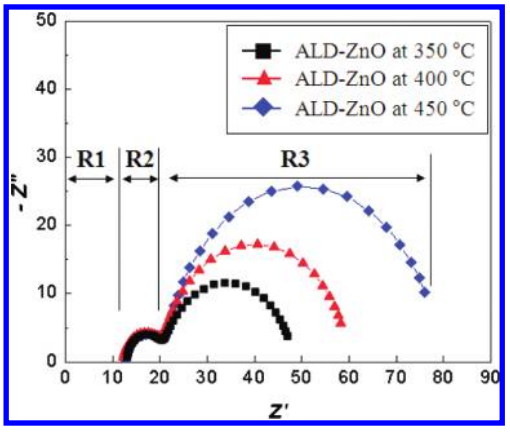

Figure 6. Nyquist plots of the ALD-TiO_2 coated ZnO aggregates annealed at 350, 400, and 450 °C.

Table 3. EIS Results of the ALD-TiO_2 Coated ZnO Aggregate Photoelectrodes Annealed at 350, 400, and 450 °C for Charge Transfer Resistances

	R2	R3
ALD-ZnO − 350 °C	7.5 Ω	27.4 Ω
ALD-ZnO − 400 °C	8.1 Ω	39.4 Ω
ALD-ZnO − 450 °C	8.4 Ω	56.8 Ω

350, 400, and 450 °C was tested under illumination with 100 mW cm^{-2} intensity. The results were shown in Figure 7 as a form of current density−voltage ($J-V$) curve and summarized in Table 4. Overall conversion efficiency (η) and fill factor (FF) were calculated according to the relationships $\eta = J_{max}V_{max}/P_{in} \times 100$ and FF = $J_{max}V_{max}/J_{sc}V_{oc}$, where J_{max} and V_{max} are maximal photocurrent density and photovoltage in the $J-V$ curve, P_{in} is the illumination power density and J_{sc} and V_{oc} are short circuit current density and open circuit density.

It is obvious that V_{oc} was increased with the annealing temperature due to the increased charge transfer resistance, which makes it difficult to the occurrence of recombination at the aggregate/electrolyte interface. V_{oc} can be expressed as follows under illumination condition;[29]

$$V_{oc} = \frac{AkT}{q} \ln\left[\frac{K_\Phi}{K_1 n_0 |I_3^-|^m + K_2 n_0 |D^+|}\right] \quad (2)$$

where A and K are constants, Φ is incident photon flux, K_1 and K_2 are kinetic constants, n_0 is electron concentration in the conduction band of the ZnO, m is reaction order and I_3^- and D^+ are concentration of I_3^- and oxidized dye molecule. In eq 2, as the terms, $k_1 n_0 |I_3^-|$ and $k_2 n_0 |D^+|$, denote the recombination with the I_3^- and oxidized dye molecule respectively, it is easily inferred that V_{oc} depends logarithmically on the recombination inversely and can be increased through reducing recombination. As notified in the EIS results, the charge transfer resistance (R3), which indicates how difficult the back flow of electrons in the conduction band of the ZnO to the I_3^- and oxidized dye molecules is under bias voltage, was increased with the annealing temperature so that the improvement of V_{oc} was observed as a result of the reduced recombination.

Coating a shell layer on the surface of the core is considered to suppress recombination by forming a surface energy barrier. This

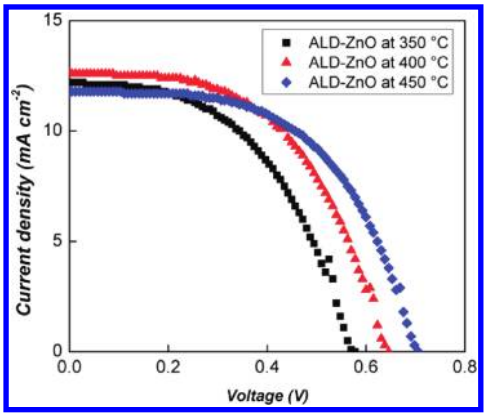

Figure 7. J-V curves of the DSCs with ALD-TiO_2 coated ZnO aggregate electrodes annealed at 350, 400, and 450 °C, respectively. All DSCs were sensitized with N719 and tested under simulated AM 1.5.

Table 4. Performances of the DSCs with the Electrode of ALD-TiO_2 Coated ZnO Aggregates Annealed at 350, 400, and 450 °C

	V_{oc} [V]	J_{sc} [mA cm^{-2}]	FF	η [%]
ALD-ZnO − 350 °C	0.578	12.2	0.49	3.5
ALD-ZnO − 400 °C	0.646	12.6	0.54	4.4
ALD-ZnO − 450 °C	0.706	11.8	0.55	4.6

effect would be achieved when the shell layer would act as an energy barrier layer or a tunneling layer depending on the energy level of the shell materials or passivate recombination sites on the surface of the core. In the ZnO core-TiO_2 shell system, as the both materials have a similar energy level, the TiO_2 shell could not form a surface energy barrier in terms of energy level.[30,31] However, it is possible to form a n−n^+ heterojunction at the ZnO/TiO_2 interface due to the difference in the electron concentration; high electron concentration in ZnO and low electron concentration in TiO_2. It is known that the electron concentrations are on the order of 10^{18} cm^{-3} and 10^{10} cm^{-3} for ZnO and TiO_2.[32,33] The shell layer, in this case, is not a depletion layer since electrons do not switch their function from a minority carrier to a majority carrier. This heterojunction induces a built-in voltage as follows:[34]

$$V = \frac{kT}{q} \ln \frac{N_d^+}{N_d} \quad (3)$$

where V is a potential gradient between the core and shell due to the n−n^+ heterojunction, k the boltzmann's constant, T the temperature, q the electron charge, and N_d are the electron concentration in the ZnO core and TiO_2 shell. The built-in voltage gives rise to a strong electric field which causes electrons to be slowed down and eventually be flowed back against the concentration gradient. This leads to the increase in V_{oc} by reducing the recombination. It is known that the fill factor (FF) is determined by the internal resistance of the cell and a practical FF is always lower than the theoretical maximum one due to the presence of internal resistive losses.[35,36] As mentioned in the EIS results, there are lots of resistance sources in DSCs like the ohmic resistance (R1) and charge transfer resistance at the different interface (R2 and R3). The charge transfer resistance at the aggregate/electrolyte interface denoted as R3 in Figure 6 is

considered as a shunt resistance because it behaves like a diode on the applied bias voltage, whereas other resistances (R1 and R2) represent a series resistance.[31] Each of them affects FF as follows:[36]

$$FF = FF_0(1 - 1/R_{sh}) \quad \text{and} \quad FF = FF_0(1 - R_s) \qquad (4)$$

where FF_0 is the theoretical maximum FF, R_{sh} is a shunt resistance (R3), and R_s is a series resistance (R1 and R2), respectively. FF would be increased in the cases that R_{sh} is increased or R_s is decreased. From the EIS results, it is expected that FF of DSCs with the electrode of the ALD-TiO_2 coated ZnO aggregate would be increased with the annealing temperature because R3 as the R_{sh} was increased with the annealing temperature, without the change in R_s. The highest FF was achieved when the annealing temperature was 450 °C, as shown in Table 4.

The trend of the change in short circuit current density (J_{sc}) was not straightforward. J_{sc} increased as the annealing temperature was increased from 350 to 400 °C and fell for further increase of the annealing temperature up to 450 °C. Lots of factors like amount of adsorbed dye, charge collection and electron injection from the dye into oxide have to be considered in determining J_{sc}. Of them, even the charge collection was improved with the annealing temperature revealed by EIS results, other two factors also affect final J_{sc}. As already mentioned, the TiO_2 shell annealed at 350 °C would be amorphous and the amorphous TiO_2 shell is known to be inefficient for the electron injection and shows the low J_{sc}.[10] The presence of the amorphous shell on the surface of the ZnO aggregate would damage the electron injection from dye molecules and this causes the current drop. However, due to the thin thickness of the TiO_2 shell layer, the damage to J_{sc} was not severe. The falloff of J_{sc} was just 8% by introducing the amorphous TiO_2 shell, comparing to that of the DSC with the ZnO aggregate electrode. With increasing the annealing temperature up to 400 °C, the TiO_2 shell transformed to a crystalline one and played a role of the barrier layer in preventing the recombination. The transformed crystalline TiO_2 would be much favorable for the electron injection from the dye molecules and also, the increased charge transfer resistance improves the charge collection by reducing the recombination and finally this combined effect recovered the J_{sc}. So, the ALD-TiO_2 coated ZnO annealed at 400 °C showed higher J_{sc} than the one annealed at 350 °C. However, the improved J_{sc} of the crystalline ALD-TiO_2 coated ZnO was still a little lower than that of the uncoated ZnO aggregate annealed at 350 °C. It seems that the ALD-TiO_2 shell impairs electron injection from dye molecules. Such a barrier effect on the electron injection was often observed in core−shell systems.[37,38] Further increase in the annealing temperature caused the loss in J_{sc}. As shown in Table 1, the fall back of J_{sc} might arise from the low light harvesting as a result of the reduced surface area and smaller dye loading. Even a slight reduction in J_{sc} was observed, the highest efficiency of DSCs was achieved at the highest annealing temperature due to the improved V_{oc} and FF resulting from the suppressed recombination.

CONCLUSIONS

The ALD-TiO_2 shell acting as surface energy barrier plays a great role in preserving the surface area of the ZnO aggregate core so that the annealing temperature at 450 °C can be applicable without a loss of the surface area. From the BET analysis on pores existed in the ZnO aggregate, it is obvious that the presence of the TiO_2 layer on the ZnO retards the diffusion of ZnO surface atoms against increasing annealing temperature. The high annealing temperature to the ZnO-TiO_2 core−shell structure causes the increase in the charge transfer resistance at the aggregate/electrolyte interface, which would expect that the recombination is decreased. As expected, the open circuit voltage as well as fill factor of the DSCs are increased due to the reduced recombination resulting from the increased charge transfer resistance with the annealing temperature and eventually the highest efficiency of the cell is obtained when the annealing temperature is 450 °C even though there is some loss in the short circuit current density.

ASSOCIATED CONTENT

Supporting Information. XPS compositional analysis of the ALD-TiO_2 coated ZnO aggregate, XRS patterns of submicrometer-sized aggregates of ZnO nanocrystallites annealed at 350 and 450 °C, equivalent circuit used to fit the Nyquist plot and performance of DSC with the electrode of submicrometer-sized aggregate of ZnO nanocrystallites annealed at 350 °C. This material is available free of charge via the Internet at http://pubs.acs.org.

AUTHOR INFORMATION

Corresponding Author
*E-mail: gzcao@u.washington.edu.

ACKNOWLEDGMENT

This work has been supported in part by the U.S. Department of Energy, Office of Basic Energy Sciences, Division of Materials and Engineering under Award No. DE-FG02-07ER46467 (Q.F.Z.), National Science Foundation (DMR-1035196), Boeing-Steiner Endowment, University of Washington TGIF grant, and Intel Corporation.

REFERENCES

(1) O'Regan, B.; Grätzel, M. *Nature* **1991**, *353*, 737.
(2) Hagfeldt, A.; Grätzel, M. *Acc. Chem. Res.* **2000**, *33*, 269.
(3) Crabtree, G. W.; Lewis, N. S. *Phys. Today* **2007**, *60*, 37.
(4) Nazeeruddin, M. K.; Kay, A.; Rodicio, I.; Humphry-Baker, R.; Muller, E.; Liska, P.; Valchopoulos, N.; Grätzel, M. *J. Am. Chem. Soc.* **1993**, *115*, 6382.
(5) Zaban, A.; Meier, A.; Gregg, B. A. *J. Phys. Chem. B* **1997**, *101*, 7985.
(6) Schlichthörl, G.; Huang, S. Y.; Sprague, J.; Frank, A. J. *J. Phys. Chem. B* **1997**, *101*, 8141.
(7) Gregg, B. A. *Coor. Chem. Rev.* **2004**, *248*, 1215.
(8) Kay, A.; Grätzel, M. *Chem. Mater.* **2002**, *14*, 2930.
(9) Nasr, C.; Kamat, P. V.; Hotchandani, S. *J. Phys. Chem. B* **1998**, *102*, 10047.
(10) Law, M.; Greene, L. E.; Radenovic, A.; Kuykendall, T.; Liphard, J.; Yang, P. *J. Phys. Chem. B* **2006**, *110*, 22652.
(11) Diamant, Y.; Chappel, S.; Chen, S. G.; Melamed, O.; Zaban, A. *Coor. Chem. Rev.* **2004**, *248*, 1271.
(12) Kim, H.; Lee, H. B. R.; Maeng, W.-J. *Thin Solid Films* **2009**, *517*, 2563.
(13) Knez, M.; Nielsch, L.; Niinisto, L. *Adv. Mater.* **2007**, *19*, 3425.
(14) Sundqvist, J.; Lu, J.; Ottosson, M.; Härsta, A. *Thin Solid Films* **2006**, *514*, 63.
(15) Ferguson, J. D.; Weimer, A. W.; George, S. M. *J. Vac. Sci. Technol. A* **2005**, *23*, 118.

(16) Park, K.; Zhang, Q. F.; Garcia, B. B.; Zhou, X. Y.; Jeong, Y.-H.; Cao, G. Z. *Adv. Mater.* **2010**, *22*, 2329.
(17) Zhang, Q. F.; Chou, T. P.; Russo, B.; Jenekhe, S. A.; Cao, G. Z. *Adv. Funct. Mater.* **2008**, *18*, 1654.
(18) Zhang, Q. F.; Chou, T. P.; Russo, B.; Jenekhe, S. A.; Cao, G. Z. *Angew. Chem., Int. Ed.* **2008**, *47*, 2402.
(19) Chou, T. P.; Zhang, Q. F.; Fryxell, G. E.; Cao, G. Z. *Adv. Mater.* **2007**, *19*, 2588.
(20) Hamann, T. W.; Martinson, A. B. F.; Elam, J. W.; Pellin, M. J.; Hupp, J. T. *J. Phys. Chem. C* **2008**, *112*, 10303.
(21) Ritala, M.; Leskelä, M.; Niinistö, L.; Haussalo, P. *Chem. Mater.* **1993**, *5*, 1174.
(22) Pierre, A. C. *Introduction to Sol-Gel Processing*; Kluwer Academic Publishers: London, 1998.
(23) Asoro, M. A.; Kovar, D.; Shao-Horn, Y.; Allard, L. F.; Ferreira, P. J. *Nanotechnology* **2010**, *21*, 025701.
(24) Dubinin, M. M.; Astakhov, V. A. *Izv. Akad. Nauk SSSR, Ser. Khim.* **1971**, *1*, 5, 11.
(25) Wang, Q.; Moser, J. E.; Grätzel, M. *J. Phys. Chem. B* **2005**, *109*, 14945.
(26) Santiago, F. F.; Biquert, J.; Belmonte, G. G.; Boschloo, G.; Hagfeldt, A. *Sol. Energy Mater. Sol. Cells* **2005**, *87*, 117.
(27) Chen, D.; Gao, Y.; Wang, G.; Zhang, H.; Lu, W.; Li, J. *J. Phys. Chem. C* **2007**, *111*, 13163.
(28) Frenck, H. J.; Kulisch, W.; Kuhr, M.; Kassing, R. *Thin Solid Films* **1991**, *201*, 327.
(29) Koelsch, M.; Cassaignon, S.; Thanh Minh, C. T.; Guillemoles, J.-F.; Jolivet, J.-P. *Thin Solid Films* **2004**, *451*−*452*, 86.
(30) Xu, Y.; Schoonen, M. A. A. *Am. Mineral.* **2000**, *85*, 543.
(31) Grätzel, M. *Nature* **2001**, *414*, 338.
(32) Studenikin, S.; Golego, N.; Cocivera, M. *J. Appl. Phys.* **1998**, *84*, 5001.
(33) Zhang, Q. F.; Dandeneau, C.; Zhou, X. Y.; Cao, G. Z. *Adv. Mater.* **2009**, *21*, 4087.
(34) Roos, O. V. *J. Appl. Phys.* **1978**, *49*, 3503.
(35) Frank, A. J.; Kopidakis, N.; Lagemaat, J. V. D. *Coord. Chem. Rev.* **2004**, *248*, 1165.
(36) Koide, N.; Islam, A.; Chiba, Y.; Han, L. *J. Photochem. Photobiol. A* **2006**, *182*, 296.
(37) Guo, J.; She, C.; Lian, T. J. *Phys. Chem. C* **2007**, *111*, 8979.
(38) Wang, Z. S.; Yanagida, M.; Sayama, K.; Sugihara, H. *Chem. Mater.* **2006**, *18*, 2912.